Climate Dynamics (2019) 52:6229–6242
https://doi.org/10.1007/s00382-018-4503-x

Assessing the internal variability in multi-decadal trends of summer surface air temperature over East Asia with a large ensemble of GCM simulations

Kaiming Hu[1,2] · **Gang Huang**[1,2] · **Shang-Ping Xie**[3,4]

Received: 14 May 2018 / Accepted: 15 October 2018 / Published online: 24 October 2018

Abstract
This study investigates the impact of internal variability on East Asian summer (June–July–August) surface air temperature (SAT) trends on the multidecadal time scale based on a 30-member ensemble of simulations that share the same external forcing from 1970 to 2005. The ensemble-mean SAT in East Asia shows a positive trend, but the patterns and the magnitudes in the individual members are remarkably diverse, highlighting the strong effect of internal variability. The first two leading empirical orthogonal function (EOF) modes of the SAT trends among ensemble members are used to represent the leading patterns of internally generated SAT change in East Asia. The first EOF mode displays a south-north dipole structure, associated with a zonally banded circulation pattern over East Asia and the North Pacific. The second mode represents coherent trend in North China, Korea and Japan, accompanied by the Northern Hemisphere annular mode (NAM)-like circulation changes. A dynamical adjustment method is applied to reduce circulation-induced internal variability in SAT, and the adjusted SAT trends are much less variable among ensemble members and more in line with the ensemble mean than the raw trends. Observed evidences show that the summertime SAT in most of East Asia, especially in northern East Asia, has experienced rapid warming in recent decades. After dynamical adjustment, the residual trends of SAT in observations are weaker than the raw trends, especially at high and middle latitudes, suggesting the enhanced warming in northern East Asia over the recent decades was not entirely anthropogenic but partly caused by internal variability.

Keywords East Asian summer surface air temperature · Internal variability · Multi-decadal trends

1 Introduction

East Asian summertime (June–July–August) surface air temperature (SAT) has experienced long-term increases over the past 100 years (Zhai et al. 1999; Li et al. 2010). Using a China Homogenized Historic Temperature dataset, Li et al. (2010) demonstrated that the best estimates of China summertime SAT trends for 1900–2006, 1954–2006 and 1970–2006 are: 0.04 ± 0.017 °C/decade, 0.16 ± 0.037 °C/decade, 0.37 ± 0.10 °C/decade, respectively. The rapid warming causes more and more hot summers in recent decades (Ding and Qian 2011; Jiang et al. 2012; Hu et al. 2013; Sun et al. 2014; Wang et al. 2014). The SAT trends in East Asia vary from region to region. Using observed data of 160 meteorological stations in China over 1951–1999, Hu (2003) reported that the summertime SAT shows remarkable increasing trends over arid and semi-arid northern China but cooling trends over central China, which was also noticed by others (Gong et al. 2004; Qian and Qin 2006). The cooling trend over central China have turn to a significant positive trend after the late 1980s (Qian and Qin 2006; You et al. 2017), meanwhile the Northeast Asia have experienced a significant warm shift (Chen and Lu 2014), suggesting that

✉ Kaiming Hu
hkm@mail.iap.ac.cn

[1] State key Laboratory of Numerical Modeling for Atmospheric Sciences and Geophysical Fluid Dynamics and Center for Monsoon System Research, Institute of Atmospheric Physics, Chinese Academy of Sciences, Beijing, China

[2] Joint Center for Global Change Studies (JCGCS), Beijing 100875, China

[3] Scripps Institution of Oceanography, University of California at San Diego, La Jolla, CA, USA

[4] Physical Oceanography Laboratory, Ocean University of China and QNLM, Qingdao, China

summertime SAT change in East Asia includes a considerable component of multidecadal variability.

The proposed factors for this multidecadal SAT change include the aerosol forcing (Li et al. 2007), greenhouse gases (He et al. 2013), sea surface temperature (SST) anomalies (Hu 2003), and atmospheric circulation adjustment (Gong et al. 2004; Wei and Chen 2011; Chen and Lu 2014). The change of aerosol and greenhouse gas should be mainly due to human activities, while SST and atmospheric circulation change are at least partly affected by internal variability of climate system (Zhou et al. 2009; Wallace et al. 2015; Song and Zhou 2015; He et al. 2017). Therefore, both human activities and natural variability appear to contribute to multidecadal SAT changes in East Asia. Internal variability could markedly modulate regional SAT trend under the increasing greenhouse gas forcing and result in large uncertainty in temperature projection (Deser et al. 2012, 2014). To obtain the anthropogenic SAT trends and reduce the uncertainty in SAT projection in East Asia, we need to understand the internal viability in the multidecadal changes of East Asian SAT.

It is often difficult to distinguish between internally-generated low frequency climate variability and human-induced climate change. Deser et al. (2012) and Wallace et al. (2012) developed a methodology to separate the forced climate change and internal variability, based on large ensemble simulations, performed with a single model, in which each member simulation starts from a different set of initial conditions and is subject to the same prescribed time-varying radiative forcing. In principle, ensemble-mean trends can be identified as externally forced climate change and the departures of the trends in the individual members from the ensemble mean are attributable to the internal variability of the climate system. In model world, this methodology works when the ensemble size is large enough to ensure a high level of statistical significance. The applicable of the methodology to real world depends upon how well the model reproduces the real climate. So, we need evaluate the skill of model before using the methodology.

Here, we investigate the effect of internal variability on summertime SAT trends in East Asia on the multidecadal time scale by using output of large ensemble simulations, following the studies of Deser et al. (2012) and Wallace et al. (2012). First, we quantify the contributions of external forcing and internal variability to the simulated SAT change in East Asia. Then, we examine the leading spatial patterns of the simulated SAT trends resulting from internal variability. Next, we analyze the corresponding atmospheric circulation, SST and rainfall anomalies to understand how the patterns are generated. Finally, we use a method to adjust the SAT trends by reducing internal variability in both simulations and observations.

The paper is organized as follows. Section 2 provides a brief description of data and methods. Section 3 evaluates the model skill in simulating East Asian climate. Section 4 quantifies the contributions of internal variability and external forcing to SAT change in East Asia. Section 5 analyzes the leading patterns of internal variability-induced SAT trends and the corresponding atmospheric circulation, SST, and rainfall changes in summer. In Sect. 6, we use a method to reduce the multidecadal internal variabilities inherent in the SAT trends for simulations and observations. Section 7 gives a summary.

2 Data and methods

A 30-member ensemble of simulations for the period of 1970–2005 by a comprehensive coupled atmosphere-ocean-sea ice-land general circulation model (GCM)—Version 4 of the Community Climate System Model (CCSM4)—at a horizontal resolution of approximately 0.94° latitude and 1.25° longitude (Wallace et al. 2015) is used to investigate the internal varbility in summer SAT multidecadal change in East Asia. Each ensemble member undergoes the same observationally estimated radiative forcing that is the same as that using in the phase 5 of the Coupled Model Intercomparison Project. All member runs start from identical initial conditions in the ocean, land and sea-ice model components, but with slightly different initial conditions in the atmospheric mode component among member runs. The detail description of the simulations is given in Gent et al. (2011).

The observed monthly SAT on grids are derived from the University of Delaware Air Temperature and Precipitation (UDel_AirT_Precip) version 4.01, available from 1901 to 2014, on a grid of 0.5° latitude × 0.5° longitude, which are provided by the NOAA/OAR/ESRL PSD, Boulder, Colorado, USA (https://www.esrl.noaa.gov/psd/). To test whether the gridded dataset is accurate enough in China, a 194-station observed monthly SAT dataset from the China Meteorological Data Service Center, China Meteorological Administration from 1970 to 2014 (http://data.cma.cn/data) is used as a comparison to the gridded observations. The gridded monthly SST is from the Hadley Centre (HadISST; available at https://www.metoffice.gov.uk/hadobs/hadisst/), with resolution of 1° × 1° (Rayner et al. 2003). The observed monthly winds and sea level pressure (SLP) are from the National Centers for Environmental prediction (NCEP) Reanalysis version 1 data (https://www.esrl.noaa.gov/psd/data/gridded/data.ncep.reanalysis.html), with a resolution of 2.5° latitude × 2.5° longitude, available from 1948 to present (Kalnay et al. 1996). The Global Precipitation Climatology Project (GPCP) 2.5° latitude × 2.5° longitude monthly precipitation dataset (https://www.esrl.noaa.gov/psd/data/gridded/

data.gpcp.html) is used to evaluate the skill of the simulations in precipitation by CCSM4, which is available from 1979 (Adler et al. 2003).

To extract the leading patterns of internal variability-induced SAT trends in East Asia, we perform empirical orthogonal function (EOF) analyses on the departures of the SAT trends from the ensemble mean using all 30 members. As the external forcing for the 30 members are exactly the same, the diversity among the 30 members should be due to internal variability. Thus, the leading EOF modes are considered as the major patterns of internally generated SAT trends in East Asia. The method to extract internal variability pattern is similar to the method used by Branstator (1990), who identified low-frequency atmospheric internal modes by performing an EOF analysis on a large ensemble of simulations forced by a number of random thermal sources. The circulation anomalies associated with the SAT EOF modes are calculated by regression onto the corresponding principal components (PCs). In this study, statistical significance is evaluated with a two-sided Student's *t* test.

3 Evaluating CCSM4 simulation over East Asia

Figure 1a, b compare the 1970–2005 climatology of June–July–August mean (JJA) land SAT in observations and the ensemble mean, respectively. The simulated and observed land SATs are similar in shape and comparable in magnitude. In both observations and the ensemble mean, high SAT above 26 °C is mainly distributed in eastern and northwest China and the Indo-China peninsula, while low SAT below 8 °C is distributed in the Tibetan Plateau. In the flat region of East Asia, SAT varies from 18 to 28 °C from

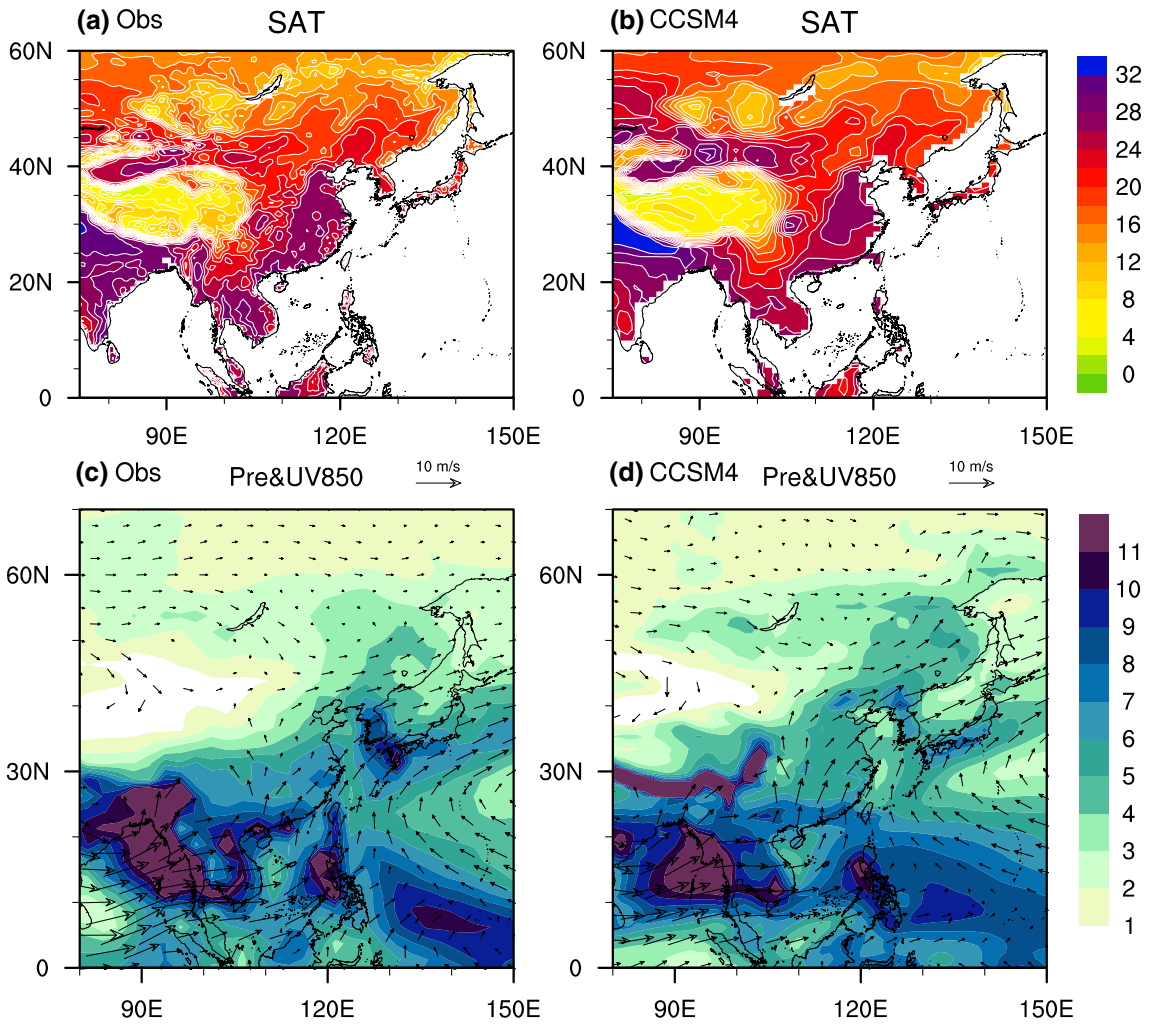

Fig. 1 The climatological JJA land SAT (the upper panels; °C), rainfall (colors in the lower panels; mm/day) and 850 hPa winds (vectors in the lower panels; m/s) in observations (left; 1979–2014) and in the ensemble mean of the 30-member CCSM4 simulations (right; 1970–2005)

the tropics to the high latitudes, a range that is much smaller than that in winter (not shown).

Figure 1c, d compare the climatological JJA rainfall and 850-hPa circulation in observations (1979–2008) and in the ensemble mean of the simulations (1970–2005). The model reproduces the southwest summer monsoon from the Indian Ocean to East Asia, southeast trades over the tropical western Pacific, an anticyclonic circulation extending from the subtropical Northwest Pacific to East China, and westerly winds at high latitudes. Dynamically consistent with circulation, there are large rainfall centers around the Bay of Bengal, the Philippine Islands and the tropical western Pacific, and the Meiyu Front that extends from East China to Japan. It is noted that the simulated Meiyu Front rainfall belt is weaker than the observed, which is generally considered hard to simulate (Kuwano-Yoshida et al. 2013). There is also a notable wet bias in the south flank of the Tibetan Plateau, consistent with a cold bias there in Fig. 1b, possibly because the model resolution is not able to make out the complex topography there. Overall, the CCSM4 shows a good skill in reproducing the observed summer climatology of 850-hPa winds, rainfall, and SAT in East Asia.

4 Internal variability vs. external forcing

Following Deser et al. (2012), the ensemble-mean SAT trends are considered as externally forced while the departures in the individual members from the ensemble-mean are due to the internal variability. We use the ratios of the ensemble-mean SAT trends to the standard deviation of departures to quantify the relative importance of external forcing and internal variability.

Figure 2 shows the JJA SAT trends in individual members. Although all members share a common prescribed forcing, the spatial patterns of SAT trends display substantial member-to-member diversity in East Asia. For example, the SAT trends feature a notable positive–negative contrast of SAT trends between southeast and northeast China in some members (#1, #4, #5 and #20), but display reverse contrast in some other members (#13, #25 and #28). The notable diversity also exists at mid and high latitudes where strong warming trends exists in some members (#2, #7, #25) but warming is weak in other members (#6, #8, #29). The large variability among ensemble members suggests that internal variability plays an important role in regional SAT trends in East Asia, consistent with the results in Yao et al. (2016).

The ensemble-mean JJA SAT trends (Fig. 3a) show robust warming everywhere. The warming rate is about 1 °C/36 years at the mid and high latitudes but below 0.5 °C/36 years in southeast China. That the warming rate is higher at the mid and high latitudes than that at low latitudes is consistent with the Artic amplification. The observed JJA SAT trends (Fig. 3b) during 1970–2005 feature large south-north gradient over East Asia, with notable warming (above 2 °C/36 years) in North China, Mongolia, and the regions around Lake Baikal but negative SAT trends (about − 0.5 °C/36 years) in the Yangtze River valley (around 30°N). The south-north dipole pattern of observed JJA SAT trends is similar to that in the members: #2, #25 and #28. The similarity lends credence to use the simulations to study internal variability in the multidecadal SAT change.

The standard deviation of the JJA SAT trends among ensemble members is quite homogeneous in East Asia (Fig. 3c). Since the ensemble-mean SAT trends are small in eastern China, the ratio of the ensemble-mean SAT trends to the standard deviation (Fig. 3d) is small there. The ratio ranges from 0.5 to 1.5 in eastern China and exceeds 2 elsewhere such as South China, the Indo-China Peninsula, the Tibetan Plateau, the Siberia, Korea and Japan. The results suggest that the effect of internal variability is on par with external forcing on summertime SAT trends in eastern China at this interval in the simulations.

5 Leading modes of internal variability

Summertime SAT trends show substantial diversity among the 30 individual members in East Asia, especially in eastern China. Does the diversity have some coherent spatial patterns? To answer the question, we perform an EOF analysis on land SAT trends among all ensemble members in the domain of East Asia (20–60°N, 90–145°E). Different domains were tested, and the results are not sensitive to the domain choice. The first and second EOF modes account for 31% and 19% of total variance of SAT trends, respectively, and are well separated from each other based on the North's criterion (North et al. 1982). Figure 4a, b display the regression maps of SAT trends upon the PC1 and PC2, respectively. For simplicity, the EOF modes shown in Fig. 4 are considered to be in their positive phase in following sections. The EOF1 displays a meridional dipole structure, with positive trends in southeast China and negative trends in northeast China and Russian Far East. The EOF2 mainly represents a broad warming in North China, Korea and Japan.

At 200 hPa, the geopotential height of EOF1 (Fig. 5a) features a meridional tripole in the sector of the North Pacific and East Asia, with negative values in the latitudinal band of 40°N–70°N and positive values on either side. In agreement with height anomalies, there are westerly wind anomalies at 200-hPa at latitudes around 40°N, indicating an enhanced subtropical jet. The regressed SLP trends (Fig. 5b) on the PC1 also show a positive-negative-positive meridional structure over East Asia and the Northwest Pacific but it shifts slightly southward relative to 200 hPa geopotential height anomalies. Rainfall anomalies are dynamically consistent

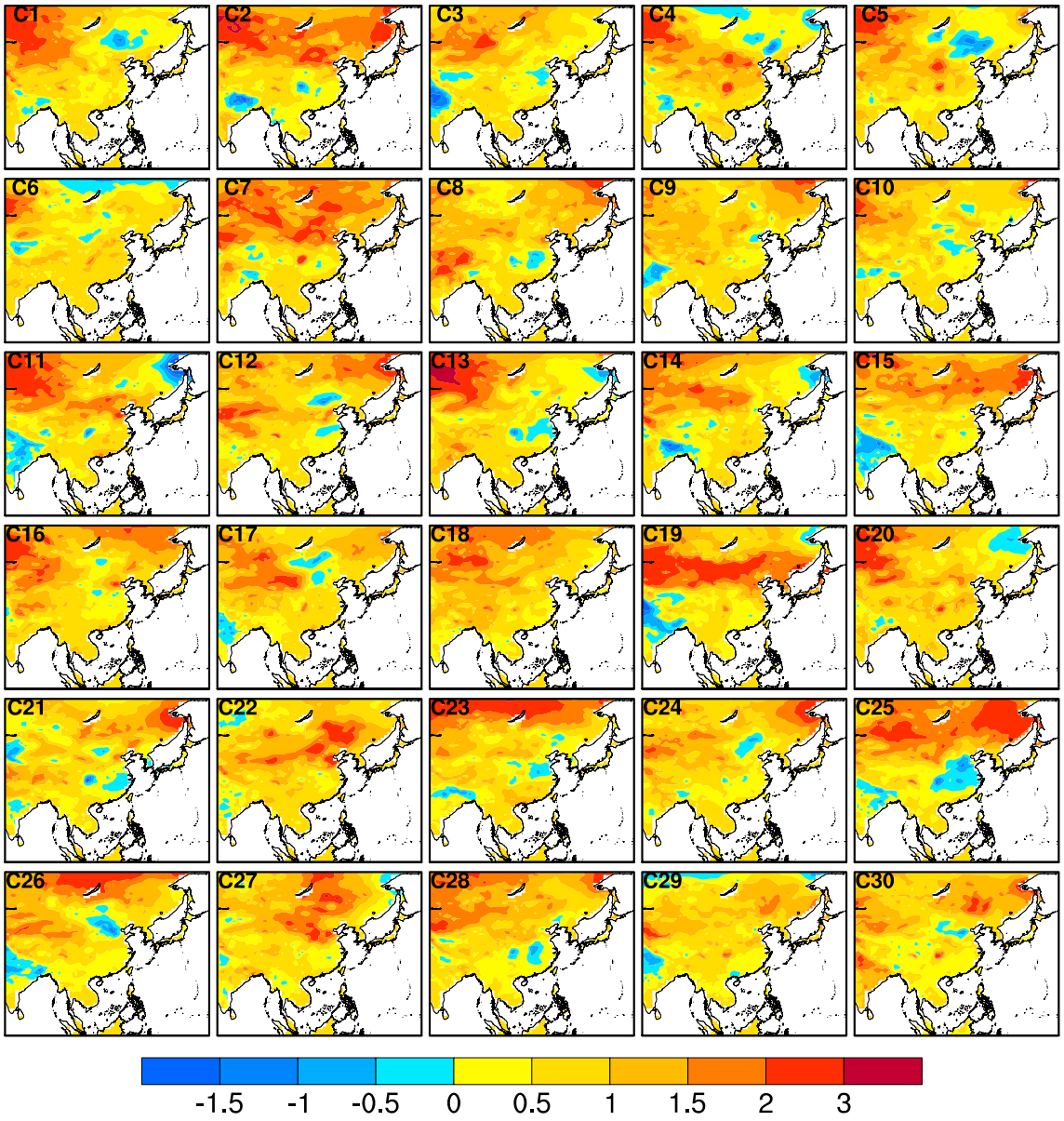

Fig. 2 JJA SAT trends (1970–2005; °C/36 year) from each of the 30 CCSM4 ensemble members

with the circulation anomalies, with negative (positive) rainfall trends (Fig. 5c) under the upper-level anticyclonic (cyclonic) circulation anomalies. In East Asia, there are negative rainfall trends in southeast China and positive rainfall trends in northeast China. A drying tendency favors warming via reduced latent heat fluxes and enhanced sensible heat fluxes at the Earth's surface, and vice versa (Hu 2003; Seneviratne et al. 2010), which corresponds to the south-north dipole structure of SAT trends in the EOF1.

Moreover, the PC1 is significantly correlated with the Pacific Decadal Oscillation (PDO; Zhang et al. 1997)-like SST trends, with warming SST trends in the tropical eastern Pacific and the tropical Indian Ocean and cooling trends in the extratropical North Pacific (Fig. 5d). The SST anomalies, especially the warming of the tropical eastern Pacific, are considered to strength the subtropical jets and lead to zonally banded circulation pattern at mid and high latitudes (Seager et al. 2003), consistent with the circulation anomalies in Fig. 5a. Using two different atmospheric general circulation models (AGCM), Li et al. (2010a, b) found that the PDO-like SST anomalies (warming in the equatorial Pacific and cooling in the subtropical North Pacific) can lead to enhanced subtropical jets at upper levels and anticyclonic-cyclonic dipole of circulation anomalies from the subtropical Northwest Pacific to the mid-latitudes at low levels. The AGCM simulated results are consistent with the circulation

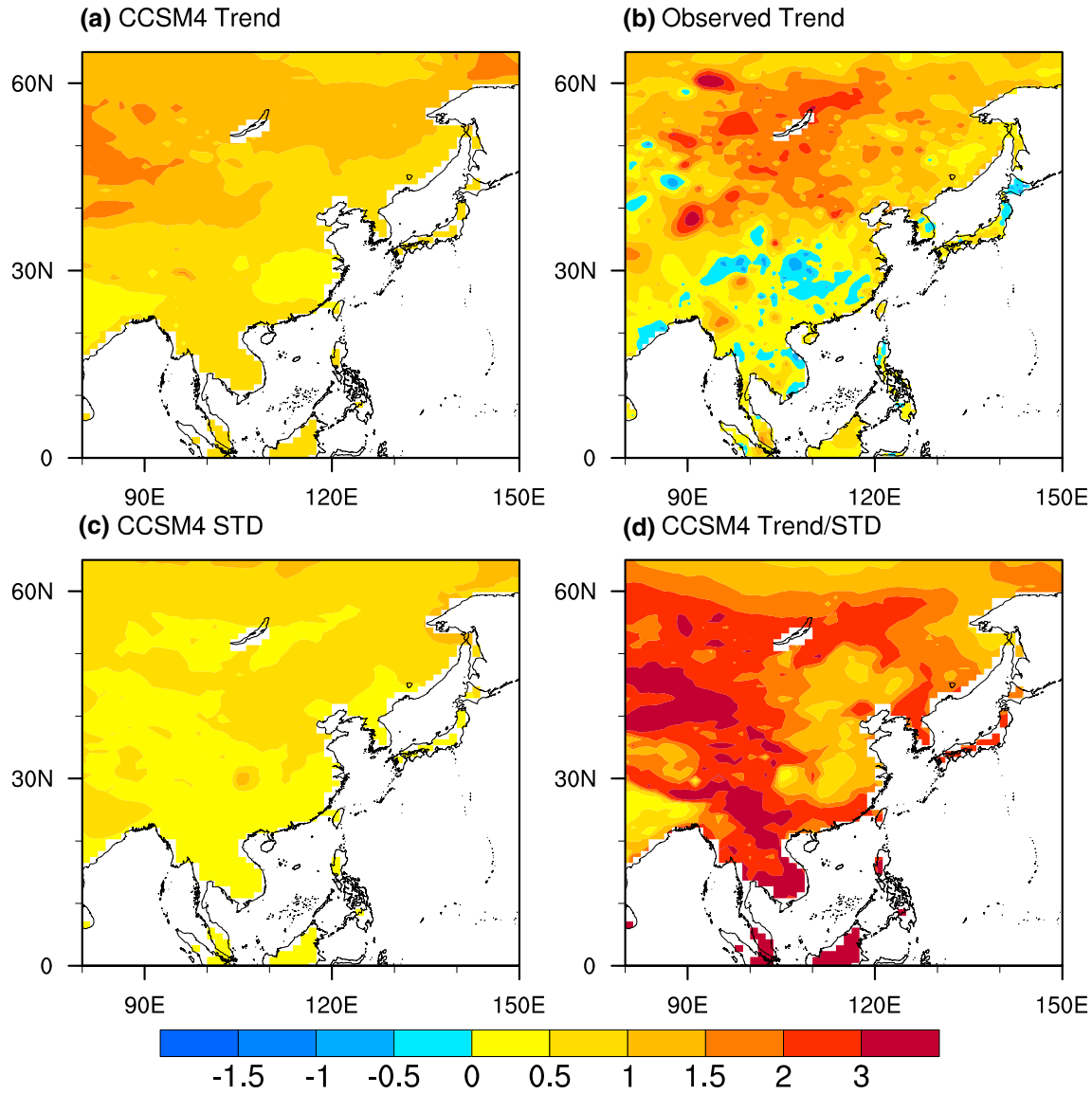

Fig. 3 **a** The ensemble-mean and **b** the observed STA trends during 1970–2005 (°C/36 year). **c** The standard deviation of the SST trends among the 30 CCSM4 ensemble members. **d** The ratio of the ensemble mean to the standard deviation of land SAT trends

anomalies shown in Fig. 5a, b. The relation between the anticyclonic-cyclonic dipole of circulation anomalies over East Asia and the Northwest Pacific and PDO-like SST pattern was also found in observations (Hu 1997; Zhou et al. 2009; Qian and Zhou 2014). The result suggests that the EOF1 of SAT trends is likely associated with the PDO.

The 200 hPa geopotential height trends associated with the EOF2 mode (Fig. 6a) display a tripole annular structure, with negative anomalies along the latitudes around 60°N and positive anomalies on either side. The tripole annular structure is more evident in SLP trends (Fig. 6b). The pattern of the circulation anomalies resembles the Northern Hemisphere annular mode (NAM), which is generally considered as an internal mode of atmospheric circulation variability (Thompson and Wallace 2000). In East Asia, the regions of North China, Korea and Japan are dominated by local upper-level anticyclonic circulation trends. Consistent with the circulation trends, there are significant negative rainfall trends in most of the polar cape regions, positive rainfall trends in the high latitudes around 60°N, and negative rainfall in North China, Korea and Japan (Fig. 6c). Compared to the SST anomalies associated with the EOF1, the EOF2-related SST anomalies (Fig. 6d) are weak and not well organized spatially, suggesting that the EOF2 mode is likely due to atmospheric internal variability.

The results indicate that the diversity of SAT trends among the 30-member ensemble is organized into some coherent patterns, with large-scale atmospheric circulation

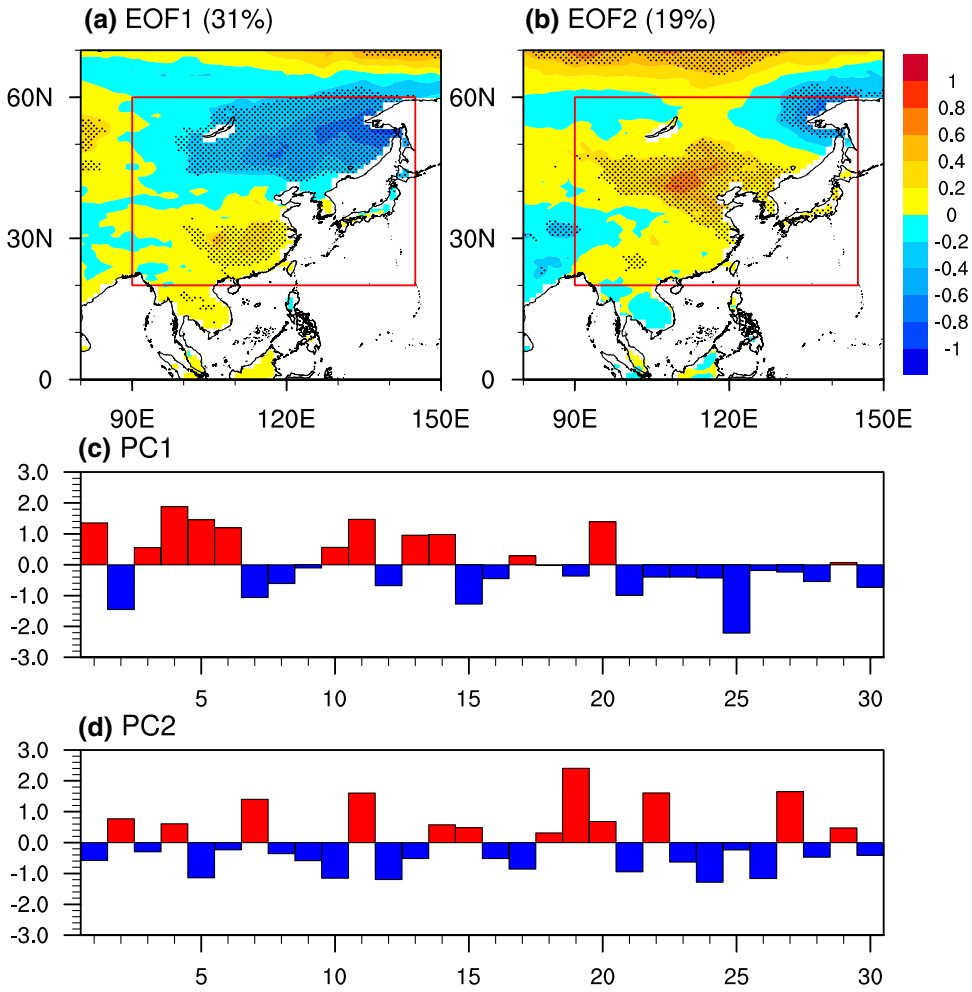

Fig. 4 Regressions (**a, b**) of SAT trends (colors; °C/36 year) among the 30 ensemble members upon the normalized PC1 (**c**) and PC2 (**d**) of EOF modes of land SAT trends in the domain of East Asia (20–60°N, 90–145°E) in summer, respectively. The EOF1 and EOF2 account for 31% and 19% of variance of SAT trends, respectively. The dots represent passing the 95% confidence level

changes. How do the circulation anomalies affect the SAT trends? It is noted that the cyclonic (anticyclonic) circulation anomalies associated with EOF1 and EOF2 are generally accompanied by positive (negative) rainfall trends. The dynamical consistency indicates that the change of circulation can lead to rainfall anomalies. The rainfall anomalies, in turn, can affect land SAT by altering soil moisture, especially in semi-arid regions where the ratio of latent and sensible heat flux largely depends on soil moisture (Mueller and Seneviratne 2012). The decrease (increase) of rainfall may lead to warming (cooling) trend. Indeed, the JJA SAT trends are negatively correlated with the simultaneous rainfall trends among the 30-member ensemble in much of East Asia (Fig. 7), consistent with the results in Wu et al. (2013). Therefore, the large-scale circulation changes can affect summertime SAT trends through modifying rainfall. The observed cooling (warming) trends in Yangtze River valley are also associated with wetting (drying) trends there (Hu 2003; Li et al. 2015).

6 Adjustment of summer multidecadal SAT trends

The above results show that the spatial patterns and magnitudes of regional summer SAT trends in East Asia in the simulations are strongly affected by internal variability, which can obfuscate the anthropogenically forced signal. Reducing the internal variability in the SAT trends helps isolate and better understand anthropogenic climate change. Noting that much of the internally generated variability in SAT is mediated by changes in the atmospheric circulation, Wallace et al. (2012) developed a method to reduce internal variability by removing the part of SAT trends related to large-scale circulation changes. Briefly, a few leading orthogonal SLP trend predictor patterns are determined for SAT trends at each grid box using the partial least squares method. Figure 8 shows the ratio of the ensemble mean to the inter-ensemble standard deviation of

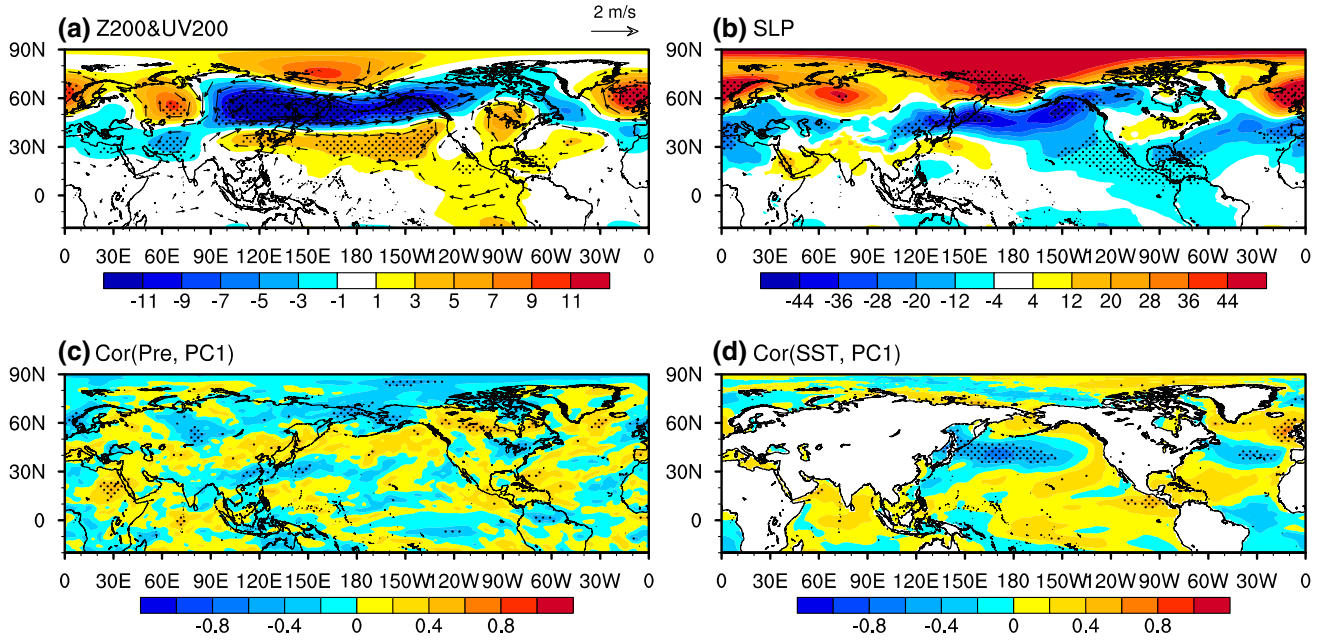

Fig. 5 Regression of JJA geopotential height trends (colors in **a**; m/36 year) and wind trends (vectors in **a**; m/s/36 year) at 200-hPa and SLP trends (**b**; Pa/36Yr) on the normalized PC1. Correlation of JJA rainfall trends (**c**) and SST trends (**d**) with the PC1. The dots and vectors represent passing the 95% confidence level

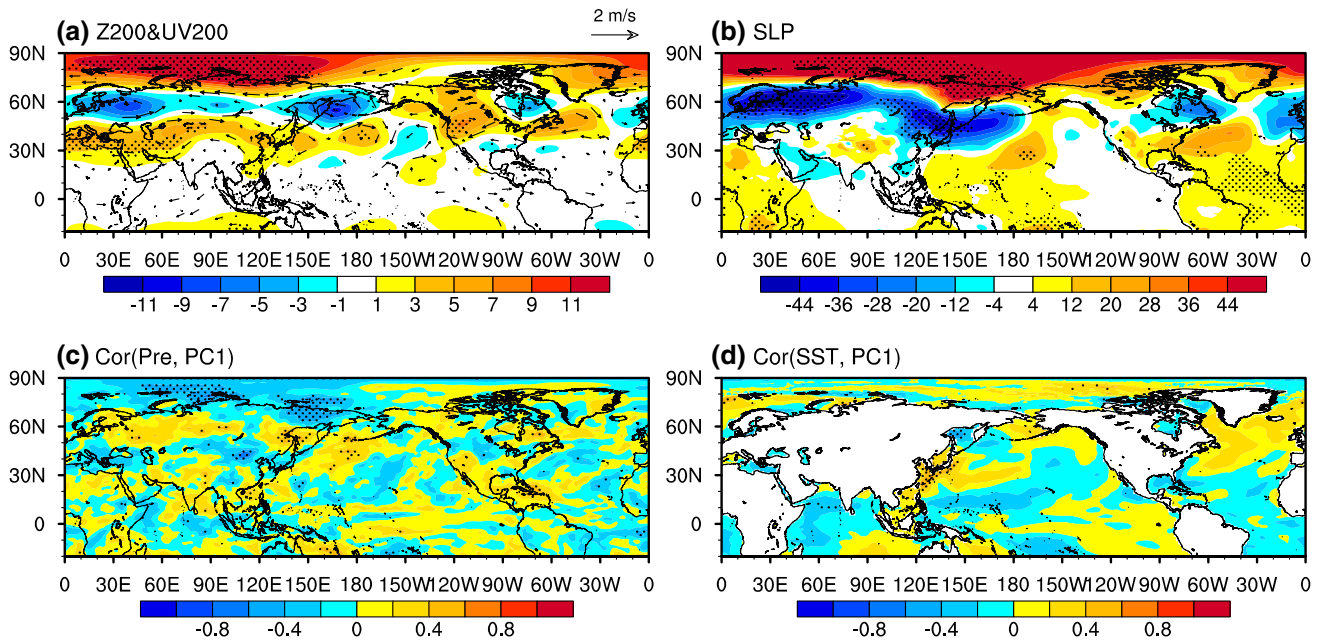

Fig. 6 As in Fig. 5 but for the PC2

SLP trend during 1970–2004 among all the 30 ensemble members. The ratio is smaller than 0.4 in much of East Asia except in part of the Tibetan Plateau and Northwest China, indicating that simulated atmospheric circulation change in each ensemble member is dominated by internal variability. Thus, the dynamical adjustment method is applicable to use here.

We use two SLP trend predictors to adjust the simulated SAT trends by the following steps. First, we regress the standardized SLP trend field upon the SAT trends $T(n)$ at

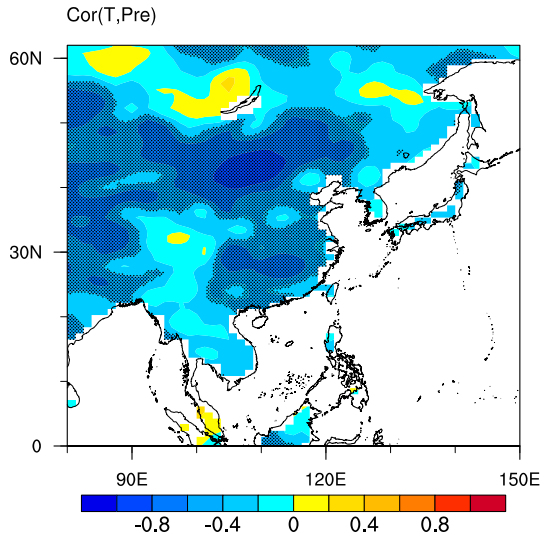

Fig. 7 Correlation between JJA rainfall trends and land SAT trends among the 30 ensemble members in every grid. The dots represent passing the 95% confidence level

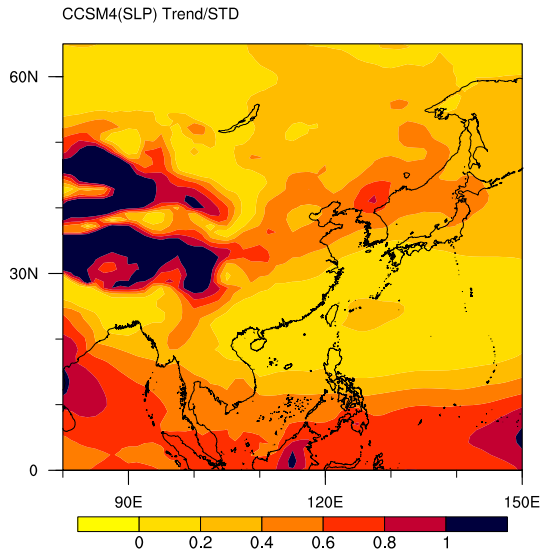

Fig. 8 The ratio of the ensemble mean to the inter-ensemble standard deviation of the JJA SLP trends over 1970–2005 in the 30-member CCSM4 ensemble simulations

a specified grid point to obtain a one-point regression map. Here, n is the sequence of the ensemble member and the standardization at each grid point is performed using all 30 members. We use the one-point regression map as a SLP predictor pattern for SAT trends at this specified grid point. Second, we project the standardized SLP trend field in each ensemble member upon the one-point regression map in the domain 10°N–80°N and 70°E–180°E to obtain a score array S(n) using the method of pattern regression. The score array S(n) provides a relative measure of the polarity and strength with which the predictor pattern is expressed in that ensemble member. Third, we compute the residual T_1(n) and SLP trends by removing the linear component associated with the S(n) using the least squares method. We repeat the above three steps on the residual T_1(n) and SLP trend to obtain a new residual T_2(n). In the residual T_2(n), the linear components associated with the first two leading orthogonal SLP predictors have been removed. In the following, we consider the residual T_2(n) as two-pass dynamically adjusted SAT trends. In this study, we only use two SLP trends predictors to dynamically adjust the SST trends at each grid point because variance of T(n) explained by the third predictors is quite small (not shown).

Figure 9 shows the two-pass dynamically adjusted summertime SAT trends for the 30 members. Compared to the raw trends in Fig. 2, the application of the dynamical adjustment substantially reduces the diversity of the SAT trends among ensemble members and makes the pattern of SAT trends in each member more similar to the ensemble mean. Specifically, the cold trends in southeast China in the members #2, #13, #23, #25, and #28 have been adjusted to slight warming trends, while the amplitude of strong warming trends at the mid and high latitudes in members #7, #13, #19, #23 and #25 has been reduced. We also tested other circulation predictors such as 200 hPa velocity trends to adjust the SAT trends and got a similar result (not shown). The results suggest that the two-pass dynamical adjustment is effective in reducing internal variability in summertime SAT trends in the simulations.

The observed summertime SAT trends also are accompanied by large-scale circulation changes. Figure 10a shows the JJA SAT and 200 hPa wind trends over 1970–2005 in observations. There is notable warming (above 2 °C/36 years) at mid and high latitudes and cooling in part of southern China especially in the Yangtze River valley, which is accompanied by a south-north dipole of 200 hPa cyclonic and anticyclonic circulation changes over China. The observed SAT and circulation trends spatially resemble those in the ensemble members #2, #25 and #28 (Fig. 10b–d), in which the SAT trends represent a strong south-north positive gradient of SAT trends and the 200 hPa wind trends features a south-north dipole structure as well. The similarity indicates that the observed East Asian summer SAT trends in recent decades are likely modulated by the south-north dipole of circulation anomalies.

Following Wallace et al. (2015), we apply the two-pass dynamical adjustment to the observed gridded JJA SAT trends (from UDel_AirT_Precip) in East Asia. In this case, the linear components associated with the first two SLP predictors are removed from the raw observed SAT in every summer during 1951–2014, and the trends of the residual SAT are considered as the adjusted SAT trends. The SLP predictors are in the domain 10°N–80°N and

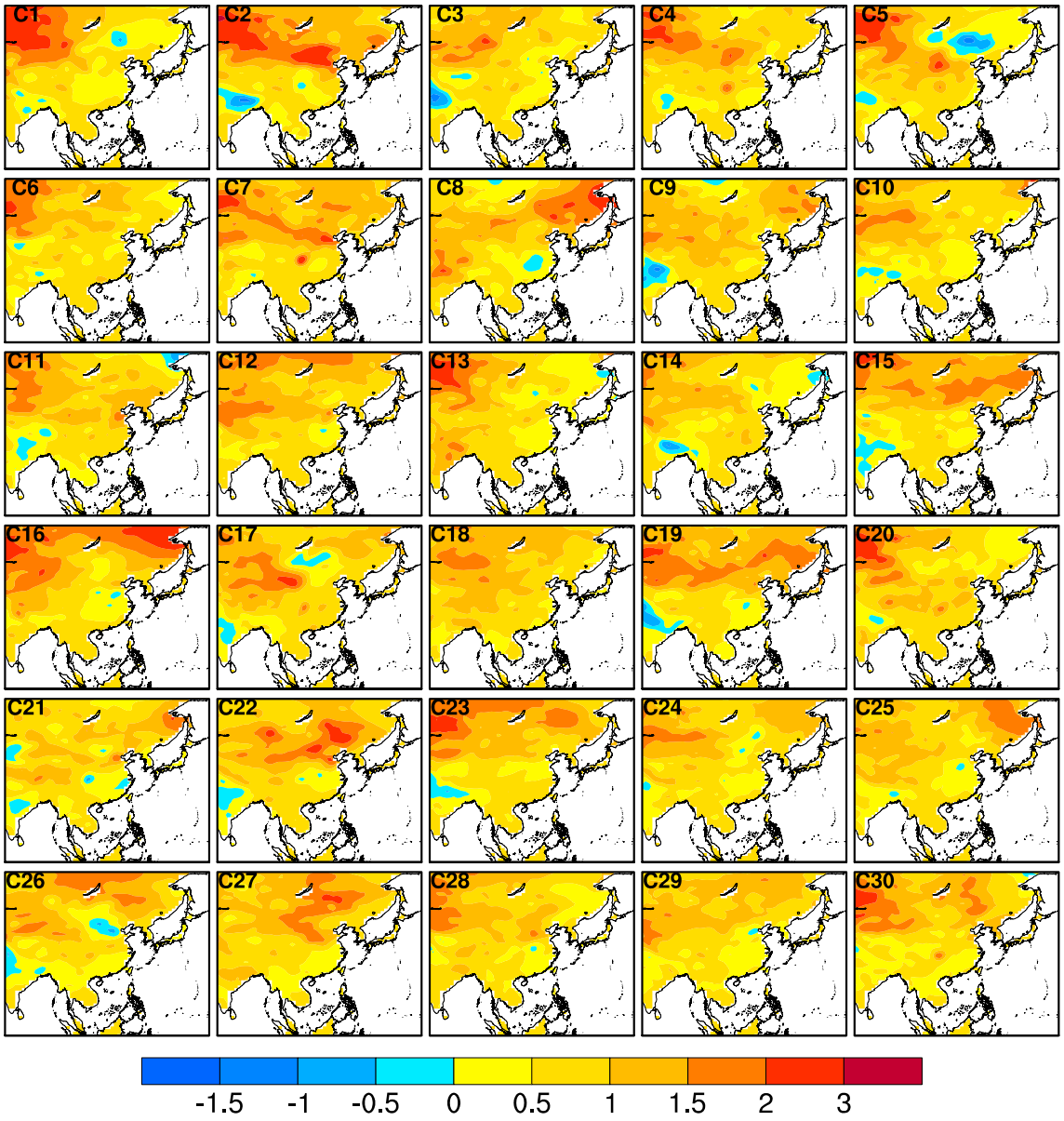

Fig. 9 The dynamically adjusted JJA SAT trends (1970–2005; °C/36 year) from each of the 30 CCSM4 ensemble members

70°E–180°E, the same as that used for the simulations. The raw and adjusted trends in the two periods: 1970–2005 and 1979–2014 are shown in Fig. 11. In raw SAT trends, there is rapid warming at middle and high latitudes in both two periods, while the cooling trend at the latitude around 30°N for 1970–2005 turn to warming trend for 1979–2014. After dynamical adjustment, the residual SAT trends are weaker than the raw trends in both two periods. The averaged warming trends in the domain 40°N–60°N, 90°E–120°E decrease from 1.62 to 1.11°C/36Yr over1970–2005 and from 1.57 to 0.99°C/36Yr over 1979–2014. The cooling in southeast China during 1970–2005 also weakens to some extent after dynamical adjustment. The adjusted SAT trends in both two periods are more in line with the ensemble mean than the raw SAT trends, likely suggesting that the dynamical adjust is useful to remove internal variability and not very sensitive to period choice. The results suggest that the observed rapid warming in northern East Asia in recent decades are partly caused by internal variability.

We also apply the two-pass dynamical adjustment to the 194-station observed JJA SAT in China. During 1970–2005 (Fig. 12a), most stations, especially in North China, experienced rapid warming except some stations in South China and Northwest China. The warming rate in North China over 1979–2014 (Fig. 12b) even become larger than that over 1970–2005. The adjusted SAT trends in most of North

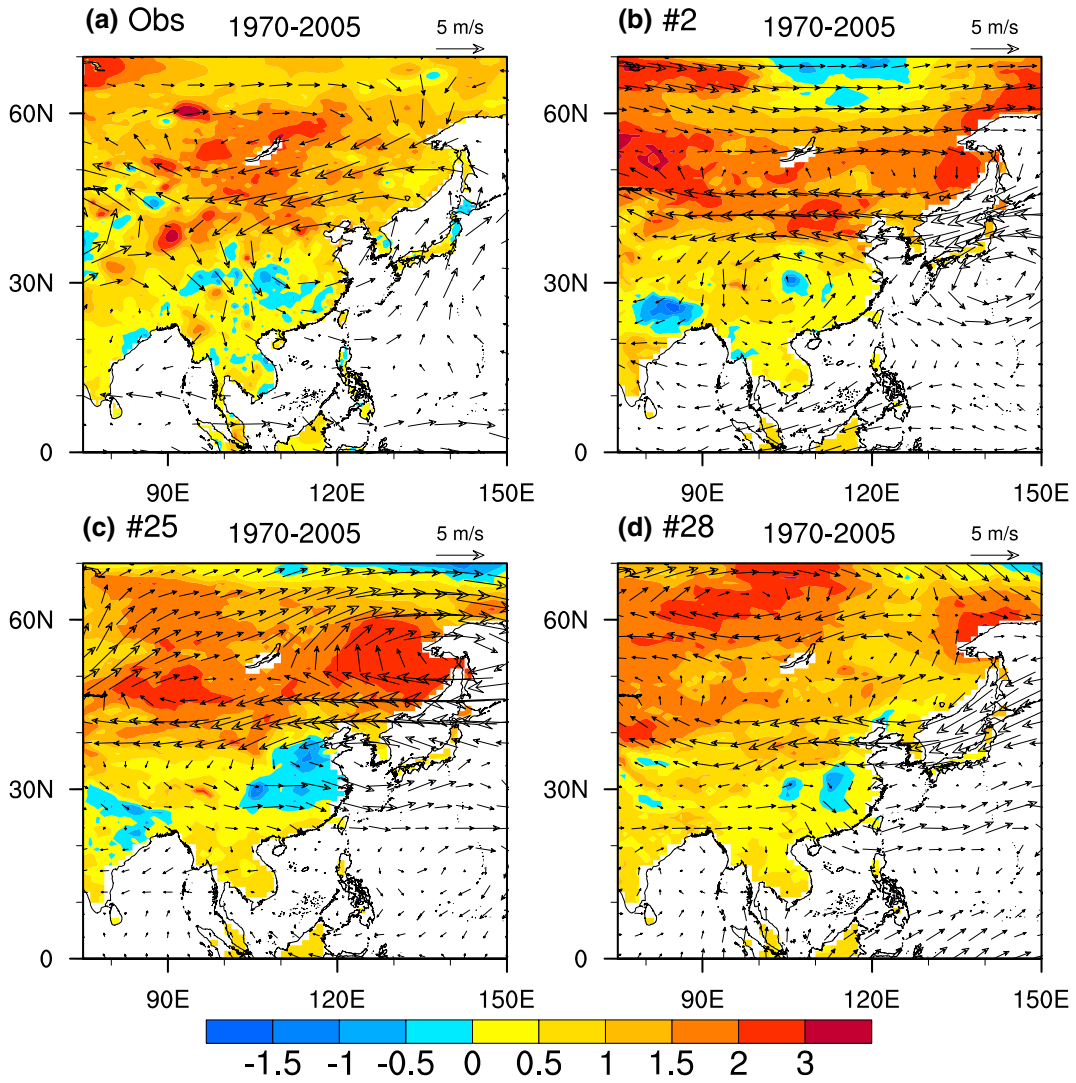

Fig. 10 JJA SAT trends (°C/36 year) and 200 hPa-wind trends (m/s/36 year) during 1970–2005 in the observations (**a**), Member #2 (**b**), Member #25 (**c**) and Member #28 (**d**)

China are weaker than the raw trends in both two periods (Fig. 12c, d). The result is similar to that based on the gridded observed SAT.

7 Summary and discussions

Using the methodology of Deser et al. (2012) and Wallace et al. (2012), we have investigated the effect of internal variability on East Asian summertime SAT trends on the multidecadal time scale based on a 30-member ensemble of simulations by CCSM4. Overall, the model can reproduce the observed climatology of 850-hPa wind, rainfall and SAT patterns well in summer. Although all members share a common prescribed radiative forcing, the summertime East Asian land SAT trend patterns in individual members are remarkably diverse, suggesting a strong influence of internal variability. The ratio of the ensemble mean to the inter-ensemble standard deviation of the JJA SAT trends mainly ranges from 0.5 to 1.5 in in eastern China, likely suggesting that the internal variability-induced SAT trends over 1970–2005 are comparable to that induced by external forcing there.

The ensemble variability of summertime SAT trends features some coherent patterns in East Asia. The first leading mode of SAT trends displays a north–south dipole structure from southeast China to Russian Far East, while the second mode represents a broad pattern of the same sign in North China, Korea and Japan. The first mode is associated with zonally banded circulation changes over East Asia and the North Pacific in both upper and low levels, which are possibly associated with PDO-like SST changes. The second

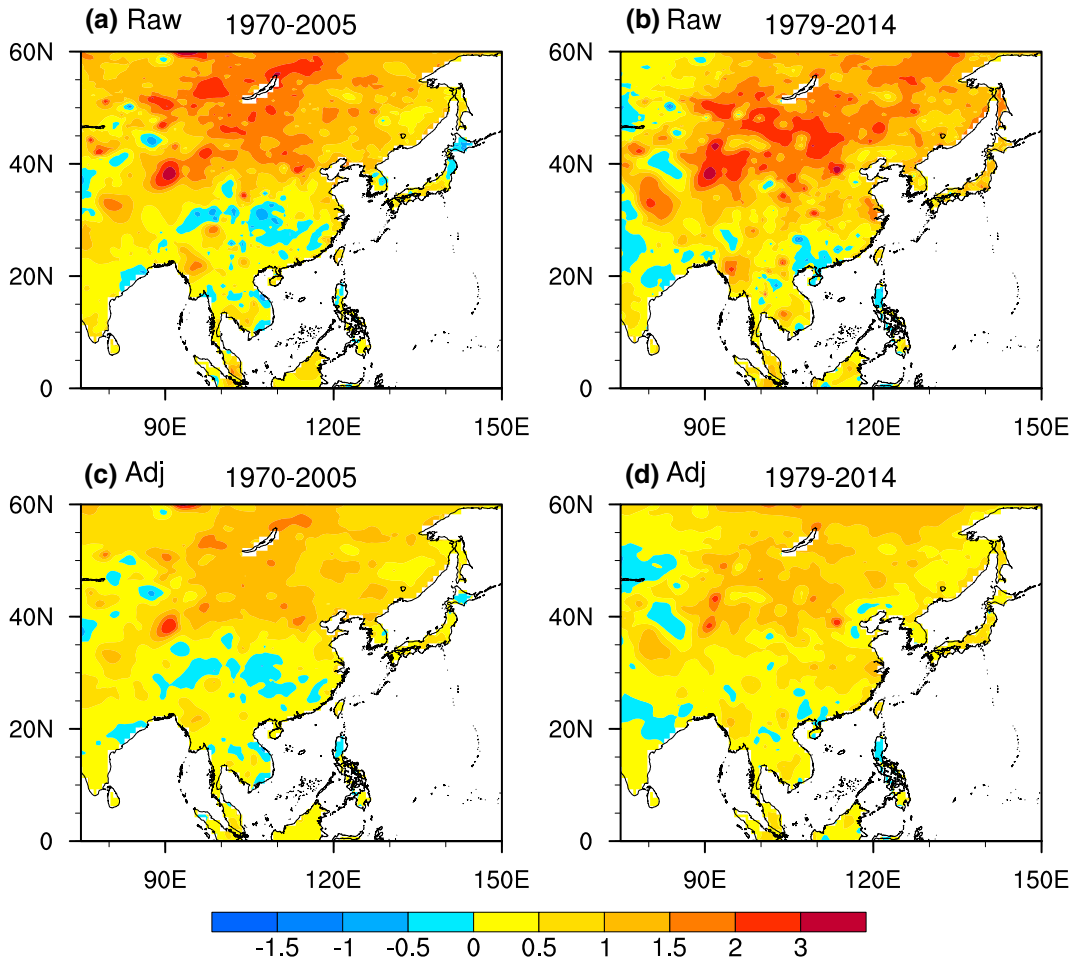

Fig. 11 The raw (upper panels) and adjusted (lower panels) SAT trends (colors, °C/36 year) in the observations during 1970–2005 (left) and during 1979–2014 (right)

mode corresponds to the NAM-like circulation changes. In general, warming (cooling) trends are accompanied by negative (positive) rainfall trends and upper-level anticyclonic (cyclonic) circulation trends.

In observations, we show that the JJA SAT trends in East Asia in recent decades are dynamically consistent with prominent atmospheric circulation changes, in agreement with previous studies (Qian and Zhu 2001; Hu 2003; Wei and Chen 2011; Chen and Lu 2014). Since the observational record is short, it is difficult to quantify the role of internal variability in East Asian JJA SAT change on the multidecadal time scale. However, the spatial resemblance of the SAT and circulation trends between observations and some ensemble members indicates that the observed East Asian summertime SAT trends in recent decades are likely modulated by large-scale circulation-induced internal variability.

A two-pass dynamical adjustment is effective in reducing internal variability in summertime SAT trends in the ensemble simulations and in observations, making them more comparable to the ensemble-mean. After dynamical adjustment, the observed warming trends at the middle and high latitudes in recent decades decreases about 30% from the raw trends, suggesting that the observed rapid warming in northern East Asia is partly caused by large-scale circulation related internal variability. The anthropogenic warming rate is likely about 1–1.1°C/36Yr in recent decades in northern East Asia, which is close to the values in the ensemble mean. Although this study focuses on SAT trends in summer, the dynamical adjustment may be also suitable to East Asian SAT trends in winter too as the wintertime SAT variations are considered to be tightly associated with large-scale circulation changes (Ma et al. 2012; Jiang et al. 2014).

We also note that the adjusted SAT trends among the ensemble members still exhibit diversity, indicating that the dynamical adjustment cannot remove all internal variability. Other factors such as time-varying soil moisture and surface heat fluxes would be capable of inducing considerable internal variability in SAT trends, even in the absence of circulation changes (Merrifield et al. 2017). In addition, anthropogenic forcing can induce changes in

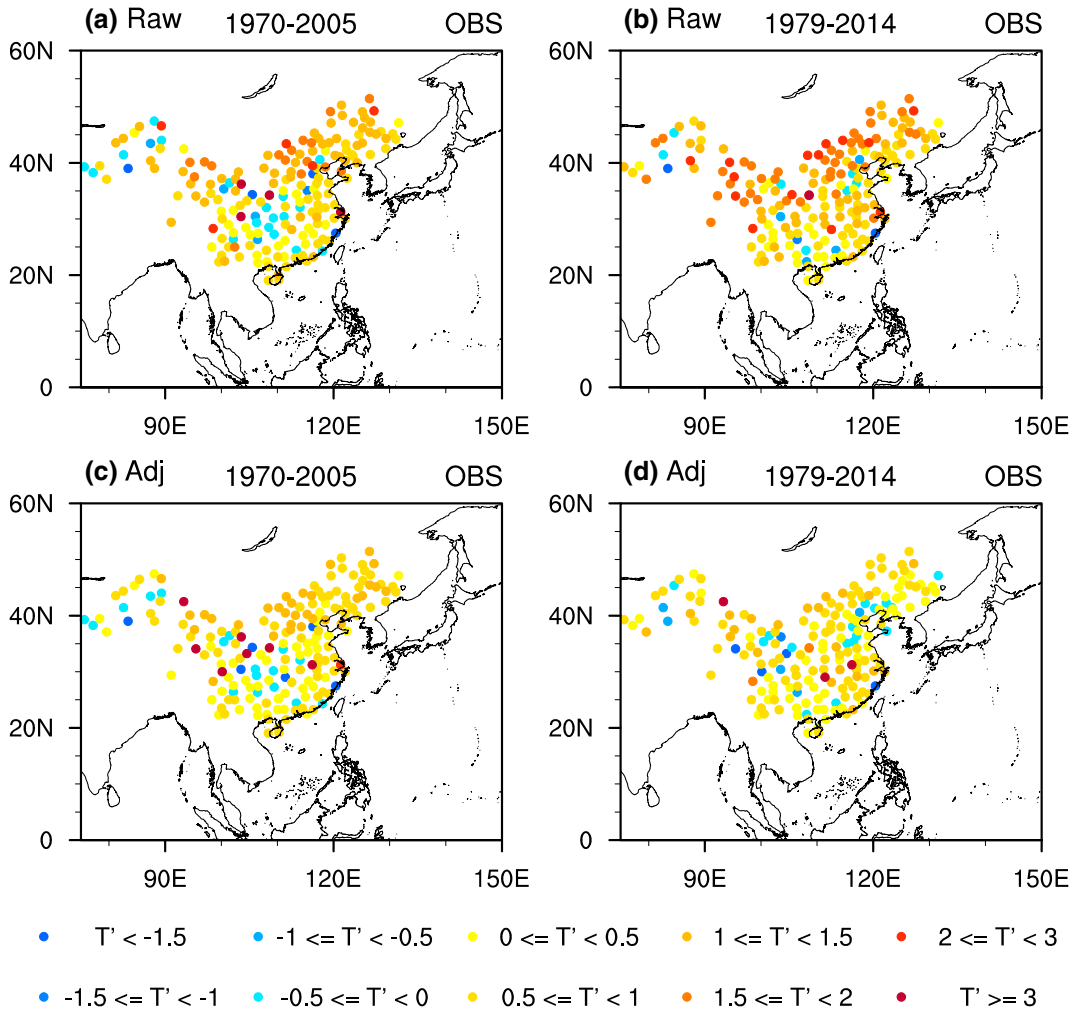

Fig. 12 The raw (upper panels) and adjusted (lower panels) SAT trends (colors, °C/36 year) in the 194-station observations in China during 1970–2005 (left) and during 1979–2014 (right)

the atmospheric general circulation. For example, aerosols could induce considerable circulation changes especially in East Asia where is a large source of emission (Li et al. 2007; Wang et al. 2016). Therefore, dynamical adjustment may remove some climate change signals caused by external forcing to some extent. Despite these caveats, this study highlights contribution of internal variability to East Asian SAT trends in the warm season and shows that the dynamical adjustment is useful in reducing the uncertainty due to internal variability.

Acknowledgements The study is jointly supported by the Strategic Priority Research Program of Chinese Academy of Sciences (XDA20060502), the National Natural Science Foundation of China (41775086 and 41661144016), the Fundamental Research Funds for the Central Universities, and State Key Laboratory of Tropical Oceanography, South China Sea Institute of Oceanology, Chinese Academy of Sciences (Project No. LTO1704). The authors declare no competing interests.

References

Adler RF et al (2003) The version-2 global precipitation climatology project (GPCP) monthly precipitation analysis (1979–Present). J Hydrometeorol 4:1147–1167

Branstator G (1990) Low-frequency patterns induced by stationary waves. J Atmos Sci 47:629–649

Chen W, Lu R (2014) A decadal shift of summer surface air temperature over Northeast Asia around the mid-1990s. Adv Atmos Sci 31:735–742. https://doi.org/10.1007/s00376-013-3154-4

Deser C, Knutti R, Solomon S, Phillips AS (2012) Communication of the role of natural variability in future North American climate. Nat Clim Change 2:775–779

Deser C, Phillips AS, Alexander MA, Smoliak BV (2014) Projecting north american climate over the next 50 years: uncertainty due to internal variability. J Clim 27:2271–2296

Ding T, Qian W (2011) Geographical patterns and temporal variations of regional dry and wet heatwave events in China during 1960–2008. Adv Atmos Sci 28:322–337

Gent PR et al (2011) The community climate system model version 4. J Clim 24:4973–4991. https://doi.org/10.1175/2011JCLI4083.1

Gong D-Y, Pan Y-Z, Wang J-A (2004) Changes in extreme daily mean temperatures in summer in eastern China during 1955–2000. Theor Appl Climatol 77:25–37. https://doi.org/10.1007/s00704-003-0019-2

He B, Bao Q, Li J, Wu G, Liu Y, Wang X, Sun Z (2013) Influences of external forcing changes on the summer cooling trend over East Asia. Clim Change 117:829–841. https://doi.org/10.1007/s10584-012-0592-4

He C, Lin A, Gu D, Li C, Zheng B, Zhou T (2017) Interannual variability of Eastern China Summer Rainfall: the origins of the meridional triple and dipole modes. Clim Dyn 48:683–696. https://doi.org/10.1007/s00382-016-3103-x

Hu ZZ (1997) Interdecadal variability of summer climate over East Asia and its association with 500 hPa height and global sea surface temperature. J Geophys Res Atmos 102:19403–19412

Hu Z-Z (2003) Long-term climate variations in China and global warming signals. J Geophys Res. https://doi.org/10.1029/2003jd003651

Hu K, Huang G, Wu R (2013) A strengthened influence of ENSO on august high temperature extremes over the southern Yangtze river valley since the late 1980s. J Clim 26:2205–2221. https://doi.org/10.1175/jcli-d-12-00277.1

Jiang Z, Song J, Li L, Chen W, Wang Z, Wang J (2012) Extreme climate events in China: IPCC-AR4 model evaluation and projection. Clim Change 110:385–401. https://doi.org/10.1007/s10584-011-0090-0

Jiang Z, Yang H, Liu Z, Wu Y, Wen N (2014) Assessing the influence of regional SST modes on the winter temperature in china: the effect of tropical pacific and Atlantic. J Clim 27:868–879

Kalnay E et al (1996) The NCEP/NCAR 40-year reanalysis project. B Am Meteorol Soc 77:437–471

Kuwano-Yoshida A, Taguchi B, Xie S-P (2013) Baiu rainband termination in atmospheric and coupled atmosphere–ocean models. J Clim 26:10111–10124. https://doi.org/10.1175/JCLI-D-13-00231.1

Li L, Wang B, Zhou T (2007) Contributions of natural and anthropogenic forcings to the summer cooling over eastern China: an AGCM study. Geophys Res Lett. https://doi.org/10.1029/2007GL030541

Li H, Dai A, Zhou T, Lu J (2010a) Responses of East Asian summer monsoon to historical SST and atmospheric forcing during 1950–2000. Clim Dyn 34:501–514

Li Q, Dong W, Li W, Gao X, Jones PD, Kennedy J, Parker DE (2010b) Assessment of the uncertainties in temperature change in China during the last century. Chin Sci Bull 55:1974–1982

Li Q et al (2015) China experiencing the recent warming hiatus. Geophys Res Lett 42:889–898

Ma T, Wu Z, Jiang Z (2012) How does coldwave frequency in china respond to a warming climate? Clim Dyn 39:2487–2496. https://doi.org/10.1007/s00382-012-1354-8

Merrifield A, Lehner F, Xie S-P, Deser C (2017) Removing circulation effects to assess central U.S. land-atmosphere interactions in the CESM large ensemble. Geophys Res Lett 44:9938–9946. https://doi.org/10.1002/2017GL074831

Mueller B, Seneviratne SI (2012) Hot days induced by precipitation deficits at the global scale. Proc Natl Acad Sci 109:12398–12403

North GR, Bell TL, Cahalan RF, Moeng FJ (1982) Sampling errors in the estimation of empirical orthogonal functions. Mon Weather Rev 110:699–706. https://doi.org/10.1175/1520-0493(1982)110%3C0699:SEITEO%3E2.0.CO;2

Qian W, Qin A (2006) Spatial-temporal characteristics of temperature variation in China. Meteorol Atmos Phys 93:1–16. https://doi.org/10.1007/s00703-005-0163-6

Qian C, Zhou T (2014) Multidecadal variability of North China aridity and its relationship to PDO during 1900–2010. J Clim 27:1210–1222. https://doi.org/10.1175/jcli-d-13-00235.1

Qian W, Zhu Y (2001) Climate change in China from 1880 to 1998 and its impact on the environmental condition. Clim Change 50:419–444

Rayner NA et al (2003) Global analyses of sea surface temperature, sea ice, and night marine air temperature since the late nineteenth century. J Geophys Res Atmos 108:4407. https://doi.org/10.1029/2002JD002670

Seager R, Harnik NI, Kushnir Y, Robinson WA, Miller J (2003) Mechanisms of hemispherically symmetric climate variability. J Clim 16:2960–2978

Seneviratne SI et al (2010) Investigating soil moisture–climate interactions in a changing climate: a review. Earth Sci Rev 99:125–161

Song F, Zhou T (2015) The crucial role of internal variability in modulating the decadal variation of the east asian summer monsoon–ENSO relationship during the twentieth Century. J Clim 28:7093–7107. https://doi.org/10.1175/jcli-d-14-00783.1

Sun Y et al (2014) Rapid increase in the risk of extreme summer heat in Eastern China. Nat Clim Change 4:1082–1085

Thompson DWJ, Wallace JM (2000) Annular modes in the extratropical circulation. Part I: month-to-month variability. J Clim 13:1000–1016

Wallace JM, Fu Q, Smoliak BV, Lin P, Johanson CM (2012) Simulated versus observed patterns of warming over the extratropical Northern Hemisphere continents during the cold season. Proc Natl Acad Sci 109:14337–14342

Wallace JM, Deser C, Smoliak B, Phillips A (2015) Attribution of climate change in the presence of internal variability, In: Chang C-P et al (eds) Climate change: multidecadal and beyond. World Scientific, Singapore, pp 1–29

Wang Y, Ren F, Zhang X (2014) Spatial and temporal variations of regional high temperature events in China. Int J Climatol 34:3054–3065

Wang H, Xie S-P, Liu Q (2016) Comparison of climate response to anthropogenic aerosol versus greenhouse gas forcing: distinct patterns. J Clim 29:5175–5188. https://doi.org/10.1175/jcli-d-16-0106.1

Wei K, Chen W (2011) An abrupt increase in the summer high temperature extreme days across China in the mid-1990s. Adv Atmos Sci 28:1023–1029

Wu R, Chen J, Wen Z (2013) Precipitation-surface temperature relationship in the IPCC CMIP5 models. Adv Atmos Sci 30:766–778

Yao S, Luo J, Huang G (2016) Internal variability-generated uncertainty in east asian climate projections estimated with 40 CCSM3 ensembles. PLOS One 11:e0149968. https://doi.org/10.1371/journal.pone.0149968

You Q, Jiang Z, Kong L, Wu Z, Bao Y, Kang S, Pepin N (2017) A comparison of heat wave climatologies and trends in China based on multiple definitions. Clim Dyn 48:3975–3989. https://doi.org/10.1007/s00382-016-3315-0

Zhai P, Sun A, Ren F, Liu X, Gao B, Zhang Q (1999) Changes of climate extremes in China. Clim Change 42:203–218

Zhang Y, Wallace JM, Battisti DS (1997) ENSO-like interdecadal variability: 1900–93. J Clim 10:1004–1020

Zhou T, Gong D, Li J, Li B (2009) Detecting and understanding the multi-decadal variability of the East Asian Summer Monsoon Recent progress and state of affairs. Meteorol Z 18:455–467